Project 1

Ivan Mak, Ethan Olson
University of Arizona
AME 554

Abstract

This paper investigates attitude regulation, attitude estimation, and controller design. Kinematic attitude regulation is successfully performed using the principle rotation vector, quaternions, and Modified Rodriguez Parameters. A single linear feedback control law is used with the principle rotation vector, where it is proven to be globally asymptotically stable. Multiple control laws are tested with many initial conditions and compared for quaternions and MRP's to validate Lyapunov stability proofs posed for each controller. It is concluded that the nonlinear control laws proposed for quaternions and MRPs are the most cost effective and eliminate problems associated with discontinuous or linear control laws. We compute the attitudes given 4 sensor measurements using both the TRIAD and OLAE methods. We then construct a series of single axis maneuvers to drive the attitude to identity at minimum cost. Finally, we apply a critically damped proportional-derivative controller that successfully tracks the nominal trajectory despite perturbations in the initial state. Control on SO(3) is performed and analyzed using a Morse-Lyapunov function and integration with a variational integrator. The controller is proven to be almost globally asymptotically stable in both simulations and the Lyapunov stability proof.

Introduction

This report investigates the design and analysis of controllers used for attitude regulation and optimal maneuvers. We discuss the Linear Time Invariant systems associated with multiple attitude descriptions, and how to develop and prove the stability of control laws for each. Next, we apply the workflow for attitude estimation and apply system dynamics to drive the system to identity along a reference and perturbed trajectory. Finally, we discuss the strengths of control and stability using a subset of 3D rotation matrices. Tasks 1 and 3 were done by Ethan Olson, and Task 2 by Ivan Mak.

The first task revolves around attitude regulation and controller design. There are three attitude descriptions of interest: Principle Rotation Vector, Q convention Quaternion, and Modified Rodriguez Parameters. Lyapunov's direct method [1] is used to develop stability proofs for each control law, which are then tested through numerical integration of the closed loop kinematics. The non uniqueness of quaternions introduces challenges in stabilizing both identity attitude presentations [2]. Three different control laws are proposed which will be analyzed in their control abilities for quaternions and whether they handle the unwinding issue. A linear and nonlinear control law are proposed for Modified Rodriguez Parameters, both of which are analyzed through Lyapunov stability. The integration of each attitude set is slightly different, the simplicity of the PRV regulation makes it ideal for MATLAB's built-in ode45. Whereas quaternions and Modified Rodriguez Parameters require the use of manual 4^{th} order Runge-Kutta integrators. The reasoning behind these integration choices is discussed further in this report.

The typical spacecraft attitude workflow first requires that the spacecraft knows its current attitude. This report discusses the TRIAD and OLAE methods of attitude determination given 4 example measurements. We discuss an example maneuver with which the spacecraft seeks to reach identity, composed of a series of single axis maneuvers. By manipulating the maneuver times for each axis, we determine the optimal lowest cost reference trajectory and input. Finally, we form a critically damped PD controller using the spacecraft inertias to track the optimal maneuver and drive the spacecraft attitude to identity despite potential errors in the initial attitude determination.

Of the three attitude parameterizations used in task 1, they all share the problem of containing either singularities or non-uniqueness. This is where the 3-D special orthogonal lie group, SO(3), comes into play. SO(3) is the space of all 3×3 rotation matrices which represent rotations about the origin in three-dimensional space [3]. Control on SO(3) directly handles the rotation matrix and does not have to deal with any of the problems associated with specific attitude representations such as quaternions or Modified Rodriguez Parameters. The stability proof of the controller is done through the analysis of a Morse-Lyapunov function, which is suitable for systems with isolated, non-degenerate critical points - including the unstable equilibria that arise in SO(3) attitude dynamics. The integration of the closed loop kinematics is performed using a variational integrator [4]. This maintains the orthogonality and properness of the rotation matrices at each timestep.

Methods

Task 1: Attitude Regulation

Task 1 consists of performing attitude kinematic feedback control using a multitude of control laws and attitude descriptions. As the name suggests, the control laws for each attitude description are developed solely based on kinematics and are independent of inertia properties. The three attitude descriptions that are of interest in this report are the principle rotation vector, q convention quaternions, and Modified Rodriguez Parameters. The goal is to drive the attitude parameters to identity attitude within 45 seconds and argue the stability of the controller using a Lyapunov function. The detailed Lyapunov proofs are given in Appendix A.

PRV

The principle rotation vector is defined as $\gamma = \Phi\hat{\boldsymbol{e}}$, where Φ is the principle angle and $\hat{\boldsymbol{e}}$ is the principle axis [5]. This parameter is not unique at rotations by π, and identity is represented by the zero vector. The kinematic differential equation is as follows:

$$\dot{\boldsymbol{\gamma}} = \left([\boldsymbol{I}] + \frac{1}{2}[\boldsymbol{\gamma}^{\times}] + \frac{1}{\|\boldsymbol{\gamma}\|^2}\left(1 - \frac{\|\boldsymbol{\gamma}\|}{2}\cot\left(\frac{\|\boldsymbol{\gamma}\|}{2}\right)\right)[\boldsymbol{\gamma}^{\times}]^2\right)\boldsymbol{\omega}$$

Equation 1: PRV KDE

Implementing the linear feedback control law, $\boldsymbol{\omega_c} = -[K]\boldsymbol{\gamma}$ where K is a scalar gain, simplifies the KDE to:

$$\dot{\boldsymbol{\gamma}} = -K\boldsymbol{\gamma}$$

Equation 2: PRV Closed Loop Kinematics

This form is very convenient to implement into ode45 and model the closed loop kinematics. To prove the stability of the closed loop kinematics, Lyapunov's direct method is used. This method is composed of the following steps [1]:

1. Given a nonlinear system $\dot{x} = f(x)$, $x(0) = x_0$, $x \in D \subseteq \mathbb{R}^n$, a reference trajectory $x_r(t) \in D$ and a Lyapunov function $V(x)$: $D \to \mathbb{R}$

1a) $V(x_r) = 0$

1b) $V(x) > 0, \forall x \in D\backslash\{x_r\}$

1c) $\dot{V}(x) = \langle\frac{\partial V}{\partial x}, f(x)\rangle \leq 0, \forall x \in D\backslash\{x_r\}$

Then $x = x_r$ is Lyapunov Stable

2. If, in addition, $\dot{V}(x) < 0, \forall x \in D\backslash\{x_r\}$ then $x = x_r$ is locally asymptotically stable.

3. If, in addition, $V(x) \to \infty$ as $\|x\| \to \infty$ then $x = x_r$ is globally asymptotically stable.

It is also important to note that a Lyapunov function is denoted a Lyapunov candidate if it only meets requirement 1a) and has continuous partial derivatives. It is denoted as a Lyapunov function if it meets requirement 1c). Using this method with the PRV closed loop kinematics, a Lyapunov candidate is proposed; $V(\gamma) = \gamma^T\gamma$. In this case, the reference trajectory is the identity attitude (i.e. an equilibrium point) which is $\gamma_I = [0\ 0\ 0]^T$. Using this information, the method can be followed using the proposed candidate to prove asymptotic stability of the identity attitude.

Lyapunov Stability Proof

$$V(\gamma_I) = 0$$

$$V(\gamma) = \gamma^T\gamma > 0, \qquad \forall\gamma \in \mathbb{R}\backslash\{\gamma_I\}$$

$$\dot{V}(\gamma) = 2\gamma^T\dot{\gamma} = -k\gamma^T\gamma < 0, \qquad \forall\gamma \in \mathbb{R}\backslash\{\gamma_I\}$$

The Lyapunov rate is negative for all values of γ besides the identity, proving local asymptotic stability. Furthermore, the Lyapunov function is radially unbounded, $\gamma \to \infty, \quad V(\gamma) \to \infty$, proving global asymptotic stability.

Quaternions

The next attitude parameter to be modeled is q convention quaternions. Quaternions involve a vector part ($\boldsymbol{q}$) and a scalar part (q_4) ($\boldsymbol{q}, q_4$) and lie on the unit 3-sphere ($S^3 \subset \mathbb{R}^4$) [2]. Quaternions do not have any singularities, however, are not unique. Two quaternions represent each attitude ($\pm q_4$), where positive q_4 typically represents the minimal rotation ($< 180°$). This means that there are two identity attitudes for quaternions, $q = [0, 0, 0, \pm 1]^T$. This introduces a phenomenon called unwinding which happens when only one of the identity attitudes is stabilized in the closed loop kinematics. Quaternions also have a unit norm constraint, $q_1^2 + q_2^2 + q_3^2 + q_4^2 = 1$. With the use of a 4th order Runge-Kutta Integrator, the quaternions can be renormalized when needed to ensure that the constraint is met throughout integration [2].

$$\begin{pmatrix} \dot{\boldsymbol{q}} \\ \dot{q}_4 \end{pmatrix} = \frac{1}{2}(\boldsymbol{\omega}, 0) \otimes q = \frac{1}{2}\begin{bmatrix} -\boldsymbol{\omega}^{\times} & \boldsymbol{\omega} \\ -\boldsymbol{\omega}^{\boldsymbol{T}} & 0 \end{bmatrix}\begin{pmatrix} \boldsymbol{q} \\ q_4 \end{pmatrix}$$

Equation 3: Quaternion KDE

The first control law being considered is a linear control law in the form $\boldsymbol{\omega} = -k\boldsymbol{q}$ where k is a scalar gain**,** and when it is plugged into the kinematic differential equation (Equation 3), the closed loop kinematics become:

$$\begin{pmatrix} \dot{\boldsymbol{q}} \\ \dot{q}_4 \end{pmatrix} = -\frac{k}{2}(\boldsymbol{q}, 0) \otimes q = -\frac{k}{2}\begin{bmatrix} -\boldsymbol{q}^{\times} & \boldsymbol{q} \\ -\boldsymbol{q}^{\boldsymbol{T}} & 0 \end{bmatrix}\begin{pmatrix} \boldsymbol{q} \\ q_4 \end{pmatrix} = -\frac{k}{2}\begin{pmatrix} q_4\boldsymbol{q} \\ -\|\boldsymbol{q}\|^2 \end{pmatrix}$$

Equation 4: Quat Closed Loop Kinematics (Linear Control)

This linear control law stabilizes the identity attitude, however only one identity attitude which causes unwinding and will be demonstrated in the results section of this report. The stability is observed through the proposed Lyapunov function $V(q) = (1 - q_4)^2 + \|\boldsymbol{q}\|^2$.

Lyapunov Stability Proof

$$V(q_I) = 0 \quad , q_I = [0, 0, 0, 1]^T$$
$$V(q) = (1 - q_4)^2 + \|\boldsymbol{q}\|^2 = 2(1 - q_4) > 0 \qquad \forall q \in S^3 \backslash (0,1)$$
$$\dot{V}(q) = -2\dot{q}_4 = \boldsymbol{\omega}_c^T\boldsymbol{q} = -k\|\boldsymbol{q}\|^2 < 0 \qquad \forall q \in S^3 \backslash (0, \pm 1)$$

The Lyapunov functions rate is negative for all values of q besides the identity and is radially unbounded, proving global asymptotic stability. However, $q = [0, 0, 0, -1]^T$ is not stabilized. This will cause unwinding when initial conditions have a negative value of q_4 and is demonstrated in the results. To fix this problem, a discontinuous control law is proposed, $\boldsymbol{\omega_c} = -k\, sgn(q_4)\boldsymbol{q}$ and if $q_4 = 0, \boldsymbol{\omega}_c = \pm k\boldsymbol{q}$**.** The closed loop kinematics become:

$$\begin{pmatrix} \dot{\boldsymbol{q}} \\ \dot{q}_4 \end{pmatrix} = -\frac{ksgn(q_4)}{2}(\boldsymbol{q}, 0) \otimes q = -\frac{ksgn(q_4)}{2}\begin{bmatrix} -\boldsymbol{q}^{\times} & \boldsymbol{q} \\ -\boldsymbol{q}^{\boldsymbol{T}} & 0 \end{bmatrix}\begin{pmatrix} \boldsymbol{q} \\ q_4 \end{pmatrix} = -\frac{ksgn(q_4)}{2}\begin{pmatrix} q_4\boldsymbol{q} \\ -\|\boldsymbol{q}\|^2 \end{pmatrix}$$

Equation 5: Quat Closed Loop Kinematics (Disc. Control)

A similar Lyapunov candidate is used to prove the stability of the control law.

Lyapunov Stability Proof

$$V(q) = (1 - |q_4|)^2 + \|\boldsymbol{q}\|^2 = 2(1 - |q_4|) > 0 \qquad \forall q \in S^3 \backslash (0, \pm 1)$$
$$V(q_I) = 0, \;\; q_I = [0, 0, 0, \pm 1]^T$$
$$\dot{V}(q) = sgn(q_4)\boldsymbol{\omega}_c^T \boldsymbol{q} = -k\|\boldsymbol{q}\|^2 < 0 \qquad \forall q \in S^3 \backslash (0, \pm 1)$$

The proof concludes that the discontinuous control law is locally asymptotically stable, and this control law will now prevent unwinding because both identity representations are stabilized. Furthermore, the Lyapunov function is radially unbounded, proving global asymptotic stability. However, discontinuous control contains its own problems, as initial conditions near $q_4 = 0$ may cause the control law to keep the attitude at the discontinuity without stabilizing it towards identity. The use of a nonlinear control law will eliminate unwinding along with the problems associated with discontinuous control. The proposed control law $\boldsymbol{\omega}_c = -kq_4\boldsymbol{q}$ gives the following closed loop kinematics.

$$\begin{pmatrix} \dot{\boldsymbol{q}} \\ \dot{q}_4 \end{pmatrix} = -\frac{kq_4}{2}(\boldsymbol{q}, 0) \otimes q = -\frac{kq_4}{2}\begin{bmatrix} -\boldsymbol{q}^{\times} & \boldsymbol{q} \\ -\boldsymbol{q}^{\boldsymbol{T}} & 0 \end{bmatrix}\begin{pmatrix} \boldsymbol{q} \\ q_4 \end{pmatrix} = -\frac{kq_4}{2}\begin{pmatrix} q_4\boldsymbol{q} \\ -\|\boldsymbol{q}\|^2 \end{pmatrix}$$

Equation 6: Quat Closed Loop Kinematics (Nonlinear Control)

Once again, a Lyapunov candidate is chosen to prove the stability of the control.

Lyapunov Stability Proof

$$V(q) = \|\boldsymbol{q}\|^2 = 1 - q_4^2 > 0 \qquad \forall q \in S^3 \backslash (0, \pm 1)$$
$$V(q_I) = 0 \qquad q_I = [0, 0, 0, \pm 1]^T$$
$$\dot{V}(q) = -2q_4\dot{q}_4 = q_4\boldsymbol{\omega}_c^T\boldsymbol{q} = -kq_4^2\|\boldsymbol{q}\|^2 < 0 \qquad \forall q \in S^3 \backslash \{(0, \pm 1), (\boldsymbol{q}, 0)\}$$

This Lyapunov function has a negative rate and is radially unbounded, proving global asymptotic stability, however it is not asymptotically stable for $q_4 = 0$, i.e. rotations of 180 degrees. Thus, the control law achieves almost global asymptotic stability.

MRP

Modified Rodriguez Parameters ($\boldsymbol{\sigma}$) have singularities at rotations of $\pm 360°$ and are unique for every attitude [6]. Like the principle rotation vector, the identity attitude is represented by the zero vector. What makes MRP's so popular is that the singularity can be avoided by switching to the shadow set ($\boldsymbol{\sigma}^S$). Commonly, the switching surface is $\boldsymbol{\sigma^2} = 1$. This can be incorporated into a 4th order Runge-Kutta integrator which will switch to the shadow set when it detects a magnitude over 1.

$$\dot{\boldsymbol{\sigma}} = \frac{1}{4}[B(\boldsymbol{\sigma})]\boldsymbol{\omega} = \frac{1}{4}[(1 - |\boldsymbol{\sigma}|^2)I_3 + 2\boldsymbol{\sigma}^{\times} + 2\boldsymbol{\sigma}\boldsymbol{\sigma}^T]\boldsymbol{\omega}$$

Equation 7: MRP KDE

The first control law proposed for regulation control is the linear feedback control law $\boldsymbol{\omega}_C = -k\boldsymbol{\sigma}$ which gives the following nonlinear closed loop kinematics.

$$\dot{\boldsymbol{\sigma}} = -k(1 + |\boldsymbol{\sigma}|^2)\boldsymbol{\sigma}/4$$

Equation 8: MRP Closed Loop Kinematics (Linear Control)

To prove stability, the following Lyapunov candidate is proposed.

Lyapunov Stability Proof

$$V(\boldsymbol{\sigma}) = 2\boldsymbol{\sigma}^T\boldsymbol{\sigma} > 0 \qquad \forall \boldsymbol{\sigma} \in \mathbb{R}^3 \backslash \{0\}$$
$$V(\boldsymbol{\sigma_I}) = 0 \qquad \boldsymbol{\sigma}_I = [0, 0, 0]^T$$
$$\dot{V}(\boldsymbol{\sigma}) = 4\boldsymbol{\sigma}^T\dot{\boldsymbol{\sigma}} = (1 + |\boldsymbol{\sigma}|^2)\boldsymbol{\sigma}^T\boldsymbol{\omega} = -k(1 + |\boldsymbol{\sigma}|^2)|\boldsymbol{\sigma}|^2 < 0 \qquad \forall \boldsymbol{\sigma} \in \mathbb{R}^3 \backslash \{0\}$$

Local asymptotic stability is proven for the identity attitude. Interestingly, if a nonlinear control law is proposed, $\boldsymbol{\omega}_c = -k\boldsymbol{\sigma}/(1+|\boldsymbol{\sigma}|^2)$, then the KDE simplifies into a linear closed loop.

$$\dot{\boldsymbol{\sigma}} = -k\boldsymbol{\sigma}/4$$

Equation 9: MRP Closed Loop Kinematics (Nonlinear Control)

The same Lyapunov function can be used to prove the stability of this control law.

Lyapunov Stability Proof

$$V(\boldsymbol{\sigma}) = 2\boldsymbol{\sigma}^T\boldsymbol{\sigma} > 0 \qquad \forall \boldsymbol{\sigma} \in \mathbb{R}^3 \backslash \{0\}$$
$$V(\boldsymbol{\sigma_I}) = 0 \qquad \boldsymbol{\sigma}_I = [0,0,0]^T$$
$$\dot{V}(\boldsymbol{\sigma}) = 4\boldsymbol{\sigma}^T\dot{\boldsymbol{\sigma}} = (1+|\boldsymbol{\sigma}|^2)\boldsymbol{\sigma}^T\boldsymbol{\omega} = -k|\boldsymbol{\sigma}|^2 < 0 \qquad \forall \boldsymbol{\sigma} \in \mathbb{R}^3 \backslash \{0\}$$

Local asymptotic stability is proven through the negative rate of the Lyapunov function. Both control laws are also radially unbounded, this means they are both globally asymptotically stable about the identity attitude.

Task 2

Task 2 involved computing the estimated attitude of a spacecraft given vectors from multiple sensor measurements. We compute the spacecraft attitude using both the Tri-Axial Attitude Determination (TRIAD) and Optimal Linear Attitude Estimator (OLAE) methods. Computing the attitude using the TRIAD method, we identify the least accurate sensor measurement.

After computing the initial attitude, we generate an optimal rest to rest maneuver that would drive the spacecraft to the identity attitude in 2 minutes. We compose this maneuver as a series of single axis maneuvers about each of the spacecraft principle axes. The system dynamics follow from the Euler Angle attitude description to simulate the nominal spacecraft attitude evolution. Finally, using the reference trajectory, the spacecraft uses a critically damped proportional-derivative controller to track the reference trajectory from a perturbed initial state.

Attitude Estimation

The spacecraft instruments output 4 different measurements for sensor pointing vectors, with known descriptions in the spacecraft body frame as well as the inertial frame. The sensor pointing vectors in the spacecraft body frame and inertial frame are given in Table 1 and Table 2.

Table 1. Sensor Pointing Vectors in Spacecraft Body Frame

Sensor	Measurement 1	Measurement 2	Measurement 3	Measurement 4
Body Frame X	0.8273	-0.8285	0.2155	0.5570
Body Frame Y	0.5541	0.5522	0.5522	-0.7442
Body Frame Z	-0.0920	-0.0955	0.8022	-0.2884

Table 2. Sensor Pointing Vectors in Inertial Frame

Sensor	Measurement 1	Measurement 2	Measurement 3	Measurement 4
Inertial Frame X	-0.1517	-0.8393	-0.0886	0.8814
Inertial Frame Y	-0.9669	0.4494	-0.5856	-0.0303
Inertial Frame Z	0.2050	-0.3044	-0.8000	0.5202

TRIAD Method

The TRIAD method of attitude determination computes a spacecraft attitude from two sensor pointing vectors that are known in the body frame and the inertial frame [7]. The first vector of the

attitude equals the most accurate pointing vector, in this case, measurement 1. A second vector is chosen arbitrarily from the remaining measurements, and a series of cross products completes the attitude direction axes in the body and inertial frames.

$$
\begin{aligned}
{}^{N,B}\hat{t}_1 &= {}^{N,B}\hat{m}_1 \\
{}^{N,B}\hat{t}_2 &= \frac{{}^{N,B}\hat{m}_1 \times {}^{N,B}\hat{m}_2}{\left|{}^{N,B}\hat{m}_1 \times {}^{N,B}\hat{m}_2\right|} \\
{}^{N,B}\hat{t}_3 &= {}^{N,B}t_1 \times {}^{N,B}\hat{t}_2
\end{aligned}
$$

Equation 10. The T frame axes are computed from sensor measurements resolved in the body and inertial frames.

The set of axes computed in Equation 10 describes the T frame resolved in the body and inertial frames. Matrix subtraction of the T frame in the two coordinate systems yields the inertial frame to estimated body frame direction cosine matrix. Thus, given measurements i and j, the resulting DCM has the form shown in Equation 11.

$$
\begin{aligned}
\left[\hat{B}T\right] &= \left[{}^{B}\hat{t}_1 \ {}^{B}\hat{t}_2 \ {}^{B}\hat{t}_3\right] \\
[NT] &= \left[{}^{N}\hat{t}_1 \ {}^{N}\hat{t}_2 \ {}^{N}\hat{t}_3\right] \\
\therefore \left[\hat{B}N_{ij}\right] &= \left[\hat{B}T\right][TN] = \left[\hat{B}T\right][NT]^T
\end{aligned}
$$

Equation 11. The T frame acts as an intermediate coordinate system, which we use to relate the estimated body frame to the inertial frame.

Given measurement 1 is the most accurate measurement, we compute 3 different attitude estimates with measurement 1 as the initial vector and measurements 2, 3, or 4 as the second vector. Each estimated attitude corresponds to a DCM describing the body frame in with respect to the inertial frame. If we compute the principle angle between two estimated attitudes per $cos\Phi = \frac{1}{2}(tr[C] - 1)$ *Equation 12* and take it as the error, the maximum error will correspond to the least accurate measurement.

$$
\begin{aligned}
[C] &= \left[\hat{B}B_{jk}\right] = \left[\hat{B}N_{1j}\right]\left[\hat{B}N_{1k}\right]^T \\
cos\,\Phi &= \frac{1}{2}(tr[C] - 1)
\end{aligned}
$$

Equation 12. Computation of principle angle errors between estimated DCM's involves their matrix subtraction.

OLAE Method

The OLAE method uses a weighted least squares fit to determine the Classical Rodriguez Parameters (CRP's) that minimizes the error with the observed measurements [7]. For each measurement, we define two vectors as the sum and difference of the observations resolved into the body and inertial frames, as in Equation 13:

$$
d_k = {}^{B}\hat{v}_k - {}^{N}\hat{v}_k, s_k = {}^{B}\hat{v}_k + {}^{N}\hat{v}_k, k = 1, \cdots, n
$$

Equation 13. We define two vectors as the sum and difference of observations resolved into

In Equation 14, we then construct a $\boldsymbol{D}$ vector from the differences and $\boldsymbol{S}$ matrix from the skew symmetric matrices of the sum vectors:

$$
\begin{aligned}
\boldsymbol{D} &= [d_1^T, d_2^T, \cdots, d_n]^T \\
\boldsymbol{S} &= \begin{bmatrix} [s_1]^\times \\ \vdots \\ [s_n]^\times \end{bmatrix}
\end{aligned}
$$

Equation 14. The sum and difference vectors for each measurement form a larger sum matrix and difference vector.

Measurement 1 is given to be twice as accurate as the other measurements. With this information, we construct a weights matrix, $\boldsymbol{W}$ in Equation 15:

$$W = \begin{bmatrix} w_1 I_{3\times3} & & \\ & \ddots & \\ & & w_n I_{3\times3} \end{bmatrix} = \begin{bmatrix} 2I_{3\times3} & & & \\ & I_{3\times3} & & \\ & & I_{3\times3} & \\ & & & I_{3\times3} \end{bmatrix}$$

Equation 15. The weights matrix is composed of a series of identity matrices multiplied by the least squares weight for each observation.

We determine the CRP vector given $\boldsymbol{D}, \boldsymbol{S}, \boldsymbol{W}$.

$$\hat{\boldsymbol{q}} = (\boldsymbol{S}^T \boldsymbol{W} \boldsymbol{S})^{-1} \boldsymbol{S}^T \boldsymbol{W} \boldsymbol{D}$$

Equation 16. The CRP is computed from the weight and sum matrices, and the difference vector.

The CRP vector relates to the DCM by the Cayleigh Transform shown in Equation 17 [6]:

$$\left[\hat{B}N\right] = (I_{3\times3} + [\boldsymbol{q}]^{\times})^{-1}(I_{3\times3} - [\boldsymbol{q}]^{\times})$$

Equation 17. The CRP vector is related to the DCM by the Cayleigh Transform.

Optimal Rest to Rest Maneuver

We compose the optimal maneuver as a series of single axis maneuvers. The optimal maneuver for a single axis is known to have a reference trajectory and a reference input of forms in Equation 18 [8]. We include the spacecraft inertias in Table 3 to compute the input signal, a torque about the given axis.

$$\theta(t) = a_1 + a_2 t + a_3 t^2 + a_4 t^3$$
$$L_g = u(t) = I\ddot{\theta}(t) = I(2a_3 + 6a_4 t)$$

Equation 18. The optimal reference trajectory for the rest to rest maneuver is a 3rd order polynomial, and the reference torque is first order.

If the spacecraft is to carry out a rest-to-rest maneuver, it must start and end the maneuver with zero velocity. Combined with an initial Euler Angle set from the OLAE estimated attitude as well as the final Euler Angle set corresponding to the identity attitude, the initial and final conditions are known. For a maneuver along a single axis, we may compute the coefficients according to Equation 19.

$$a_1 = \theta(t_0) = \theta_0, a_2 = \dot{\theta}(t_0) = 0, a_3 = \frac{3\left(\theta_f - \theta_0\right)}{\Delta t^2}, a_4 = -\frac{2\left(\theta_f - \theta_0\right)}{\Delta \mathrm{t}^3}$$

Equation 19. The coefficients of the reference trajectory and input are computed from 4 boundary conditions on the initial and final state.

However, the total maneuver must occur in 2 minutes (120 seconds). That is, $\Delta t_1 + \Delta t_2 + \Delta t_3 = 120$. There are two free variables that determine the space of available maneuvers. From this set, we seek the optimal maneuver with the lowest cost defined by summing the cost u_i of the maneuver about each individual axis i.

$$J = \frac{1}{2}\int_{t_0}^{t_f} u^2(t)dt = J(\Delta t_1, \Delta t_2) = \frac{1}{2}\int_0^{\Delta t_1} u_1^2(t)dt + \frac{1}{2}\int_{\Delta t_1}^{\Delta t_1 + \Delta t_2} u_2^2(t)dt + \frac{1}{2}\int_{\Delta t_1 + \Delta t_2}^{120} u_3^2(t)dt$$

Equation 20. The cost of each maneuver is the reference torque squared integrated over the time interval.

Solving this equation for the minimum cost J results in the set of relationships in Equation 21, the solution of which fixes the maneuver times for each axis.

$$a_3 = \frac{\psi_0 I_3}{\Delta \mathrm{t}_3^2} = \frac{\theta_0 I_2}{\Delta \mathrm{t}_2^2} = \frac{\phi_0 I_1}{\Delta \mathrm{t}_1^2}$$

Equation 21. The optimal times for each single axis maneuver are found by setting the a_3 coefficient equal for each reference input.

As a result, Euler angle and reference input time histories are known. The Euler Angle set at each epoch corresponds to a DCM, whose principle angle may be computed by Equation 12.

Table 3. Spacecraft Body Principle Inertias

Axis	1	2	3
Inertia ($kg\text{-}m^2$)	1500	1000	800

Putting it all together, we simulate the system response to the optimal rest to rest maneuver in the form of $\dot{x} = Ax(t) + Bu(t)$ according to Equation 22. The signal, $u_q(t)$ and its associated trajectory correspond to the reference input computed from the inertia and initial conditions of axis q: θ_q and I_q.

$$A = \begin{bmatrix} 0_{3\times3} & \mathbf{\Gamma} \\ 0_{3\times3} & 0_{3\times3} \end{bmatrix}, \Gamma = \frac{1}{\cos\theta}\begin{bmatrix} 0 & \sin\phi & \cos\phi \\ 0 & \cos\phi\cos\theta & -\sin\phi\cos\theta \\ \cos\theta & \sin\phi\sin\theta & \cos\phi\sin\phi \end{bmatrix}$$

$$B = \begin{bmatrix} 0_{3\times3} \\ \boldsymbol{I}^{-1} \end{bmatrix}, \boldsymbol{I} = \begin{bmatrix} I_1 & & \\ & I_2 & \\ & & I_3 \end{bmatrix}$$

$$x(t) = \left[\psi, \theta, \phi, {}^B\omega_1, {}^B\omega_2, {}^B\omega_3\right]^T$$

$$\boldsymbol{u}(t) = \begin{bmatrix} u_1(t) \\ 0 \\ 0 \end{bmatrix}, 0 \le t < \Delta t_1$$

$$\boldsymbol{u}(t) = \begin{bmatrix} 0 \\ u_2(t) \\ 0 \end{bmatrix}, \Delta t_1 \le t < \Delta t_1 + \Delta t_2$$

$$\boldsymbol{u}(t) = \begin{bmatrix} 0 \\ 0 \\ u_3(t) \end{bmatrix}, \Delta t_1 + \Delta t_2 \le t < 120$$

Equation 22. The LTI system for spacecraft attitude involves the Euler Angle KDE in the state dynamics matrix, the inertia tensor in the control matrix, and the Euler angles and body angular rates in the state.

Tracking Controller

To construct a tracking controller, we add proportional and derivative terms to the reference input, so that the input signal depends on the state as well as the maneuver time [8]. The reference trajectories for each Euler Angle and body rate may be calculated using the coefficients of the optimal rest to rest maneuver. Note that the order of the position vector, Θ, is reversed in Equation 23 so that the input entries match the corresponding state position and body rate.

$$u(t) = u_r(t) - k_p\left(\Theta - \Theta_r(t)\right) - k_d\left({}^B\Omega - {}^B\Omega_r(t)\right)$$

$$\Theta = \begin{bmatrix} \phi \\ \theta \\ \psi \end{bmatrix}, {}^B\Omega = \begin{bmatrix} {}^B\omega_1 \\ {}^B\omega_2 \\ {}^B\omega_3 \end{bmatrix}$$

Equation 23. The tracking controller input depends on the modified state vector and the body frame angular rates.

We pick the proportional gain arbitrarily and then complete the critically damped controller by setting the damping coefficient to 1 and computing the derivative gain in Equation 24.

$$k_p = \omega_n^2\boldsymbol{I}, k_d = 2\omega_n\zeta\boldsymbol{I} = 2\omega_n\boldsymbol{I}$$

Equation 24. We multiply the scalar gains by the inertia tensor to produce a torque tracking control input.

Task 3

Task 3 involved designing a controller which performs regulation control for the DCM-based Morse-Lyapunov controller on SO(3). SO(3), the 3-D special orthogonal Lie group, is the configuration manifold of a rigid body attitude which is the set of rotation matrices from the body frame to the inertial frame [3].

$$SO(3) = \{R \in \mathbb{R}^{3\times3} | R^T R = I_3 \; and \det(R) = 1\}$$
$$\dot{R} = R\boldsymbol{\omega}^{\times}$$

Equation 25: SO(3) KDE

Due to the fact SO(3) deals with the actual rotation matrix, the control is free of singularities and discontinuity. To ensure the constraints of proper orthogonality are kept during integration, a geometric variational integrator is implemented which preserves the orthogonality of the rotation matrix. The orthogonality error can also be calculated to ensure the validity of the integration. The solution of the kinematic differential equation is used to design the integrator.

KDE Solution

$$\dot{R} - R\boldsymbol{\omega}^{\times} = 0$$
$$\left(\dot{R} - R\boldsymbol{\omega}^{\times}\right)e^{-\boldsymbol{\omega}^{\times}t} = \dot{R}e^{-\boldsymbol{\omega}^{\times}t} - R\boldsymbol{\omega}^{\times}e^{-\omega^{\times}t} = \frac{d}{dt}\left(Re^{-\omega^{\times}t}\right) = 0$$
$$\int_{t_0}^{t} \frac{d}{dt}\left(Re^{-\omega^{\times}t}\right) = R(t)e^{-\omega^{\times}t} - R(t_0)e^{-\omega^{\times}t_0} = 0$$
$$R(t)e^{-\omega^{\times}t} = R(t_0)e^{-\omega^{\times}t_0}$$
$$R(t) = R(t_0)e^{\omega^{\times}dt}$$

Now that the solution has been derived, a control law can be proposed and through Lyapunov's direct method it can be analyzed, which will drive the rotation matrix to the identity matrix.

$$\boldsymbol{\omega}_c = -kS_A(R) \quad S_A(R) = \frac{1}{2}(AR - R^T A)^{\vee}$$

Equation 26: SO(3) Control Law

$S_A(R)$ is a measure of how far R is from identity, where $A \in \mathbb{R}^{3\times3}$ and is made up of three positive distinctive elements on the diagonals. The elements of the A matrix are arbitrarily chosen and in this case were chosen to be $A_{11} = 5, A_{22} = 6, A_{33} = 9$. The control can be further simplified if A is the identity matrix [3], however this is not covered in this report. The stability proof of this control law is accomplished using a Morse-Lyapunov function. A Morse function is a function with isolated, non-degenerate critical points, meaning the Hessian matrix is non-singular. In the context of SO(3), there may exist saddle points corresponding to undesired equilibria (E_n) in the Morse-Lyapunov function which are not included in the region of attraction for an asymptotically stable control law.

Lyapunov Stability Proof

$$V(R) = \frac{1}{2}tr(A - AR) > 0 \qquad \forall R \in SO(3)\backslash\{I_3, E_1, E_2, E_3\}$$
$$V(I_3) = 0$$
$$\dot{V}(R) = -\frac{1}{2}tr\left(A\dot{R}\right) = -\frac{1}{2}tr(AR\omega^{\times}) = w^T\frac{1}{2}(AR - R^T A)^{\vee} = \omega^T S_A(R)$$
$$\dot{V}(R) = -kS_A(R)^T S_A(R) < 0 \qquad \forall R \in SO(3)\backslash\{I_3, E_1, E_2, E_3\}$$
$$E_1 = R_x(180°), E_2 = R_y(180°), E_3 = R_z(180°)$$

This Morse-Lyapunov function has three unstable equilibria corresponding to reflections about the axes. These are not in the region of attraction of the controller; thus, it is proven through Lyapunov's direct method to be almost globally asymptotically stable.

Results and Discussion

Task 1

PRV

As discussed in the methods, the linear feedback control law $\boldsymbol{\omega_c} = -[K]\boldsymbol{\gamma}$ was proved through Lyapunov's direct method to be globally asymptotically stable. Meaning it should drive the attitude to identity no matter the initial conditions. To test this theory, the PRV closed loop kinematics were integrated using ode45 and an arbitrary initial condition in terms of principle angle and axis. A gain of $k = 0.45$ was chosen which ensures convergence within 45 seconds.

$$ICs: \hat{e} = [-0.3626, 0.3725, 0.8543] \quad \phi = 268°, \gamma = \phi \hat{e}$$

Equation 27: PRV IC's

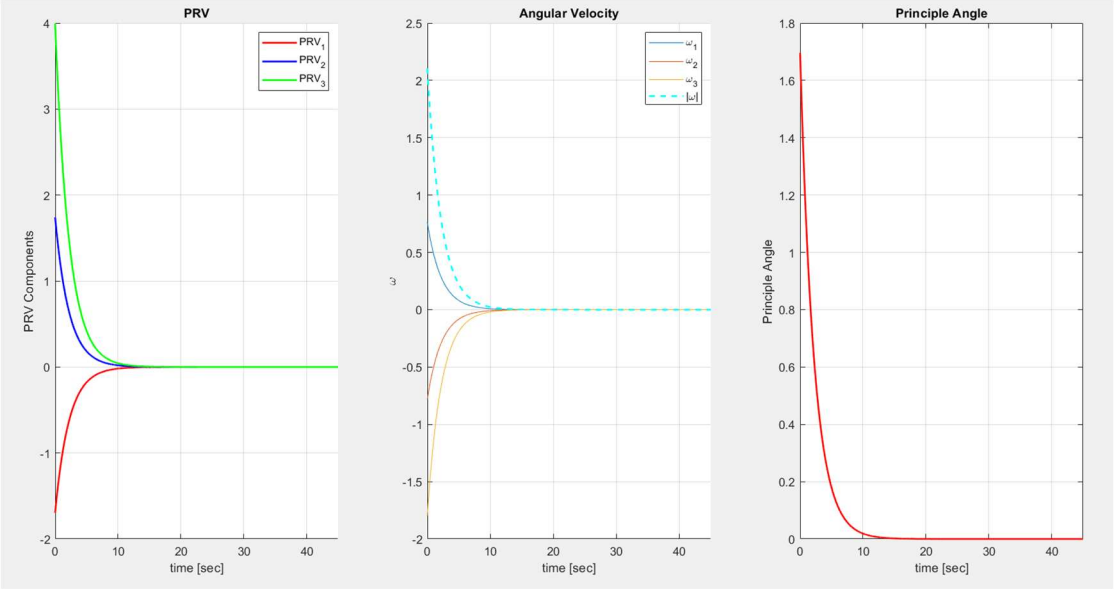

Figure 1: Linear PRV Control

Figure 1 demonstrates the stability of the identity attitude using PRV linear feedback regulation control. The trajectory stabilizes within around 15 seconds. The structure of the linear control law produces a response which reflects the PRV components about the x axis, scaled by the gain. Due to the nonsingular nature of PRVs, the simple feedback control law proves to be very effective for attitude regulation using the principle rotation vector. The stability is further tested through a range of initial rotation angles (ϕ) (Appendix B, Figure 15). The controller stabilizes each initial rotation at the identity attitude, further proving the stability of the controller.

Quaternions

Three control laws have been proposed for quaternion attitude regulation. All three closed loop kinematic equations are integrated using a 4th order Runge-Kutta integrator which preserves the unit constraint of the quaternions at each timestep. First, the linear control law $\boldsymbol{\omega} = -k\boldsymbol{q}$ was concluded to be globally asymptotically stable for $q = [0, 0, 0, 1]^T$, which presented the possibility for unwinding. Using

the same gain and initial conditions as the controller used in the PRV attitude regulation, the unwinding phenomenon can be observed.

$$q_1 = \hat{e_1} \sin\left(\frac{\phi}{2}\right) q_2 = \hat{e_2} \sin\left(\frac{\phi}{2}\right) q_3 = \hat{e_3} \sin\left(\frac{\phi}{2}\right) q_4 = \cos\left(\frac{\phi}{2}\right)$$

Equation 28: Principle Angle/Axis to Quat Transformations for IC

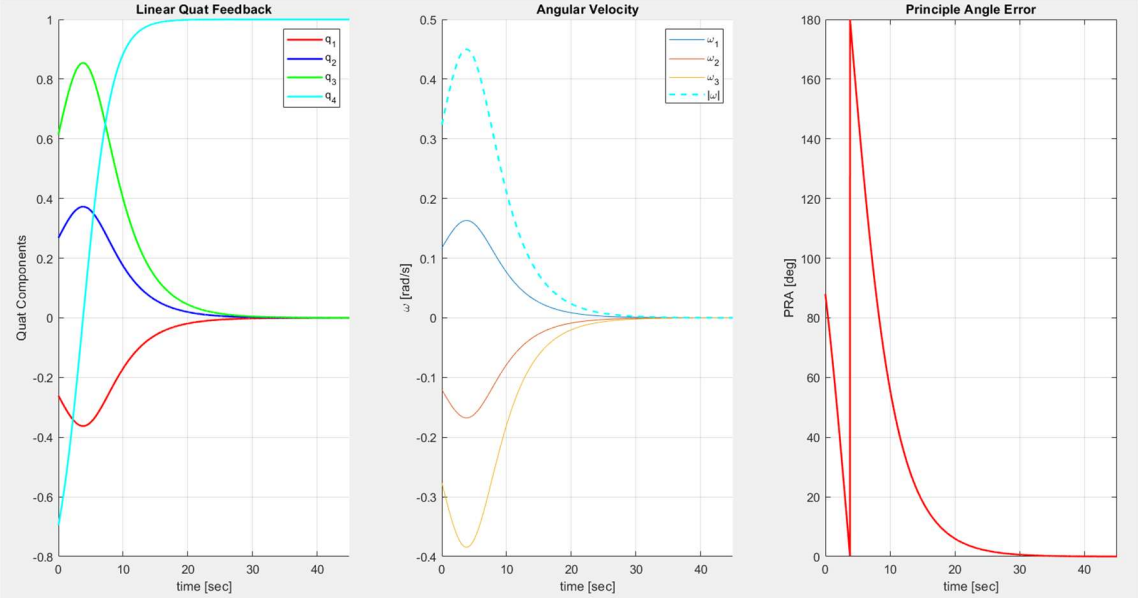

Figure 2: Linear Quaternion Control

As predicted and observed in Figure 2, the controller does not stabilize $q_4 = -1$ and instead 'unwinds' towards $q_4 = +1$, using excess control effort that otherwise would be minimized if both identity representations were stable. Clearly this would be very impractical for a real-world mission and would waste valuable energy. Similarly to the PRV control, the linear control law produces a response which is a reflection about the x axis of the vector components of the quaternion, with a magnitude difference due to the gain. As expected, larger attitude errors produce larger control efforts.

The discontinuous control law, $\boldsymbol{\omega_c} = -k\, sgn(q_4)\boldsymbol{q}$ and if $q_4 = 0, \boldsymbol{\omega}_c = \pm k\boldsymbol{q}$, is proposed to fix the problem of unwinding and stabilize both identity representations. The integration of the closed loop kinematics with the discontinuous control law uses the same initial conditions and gain as the previous cases.

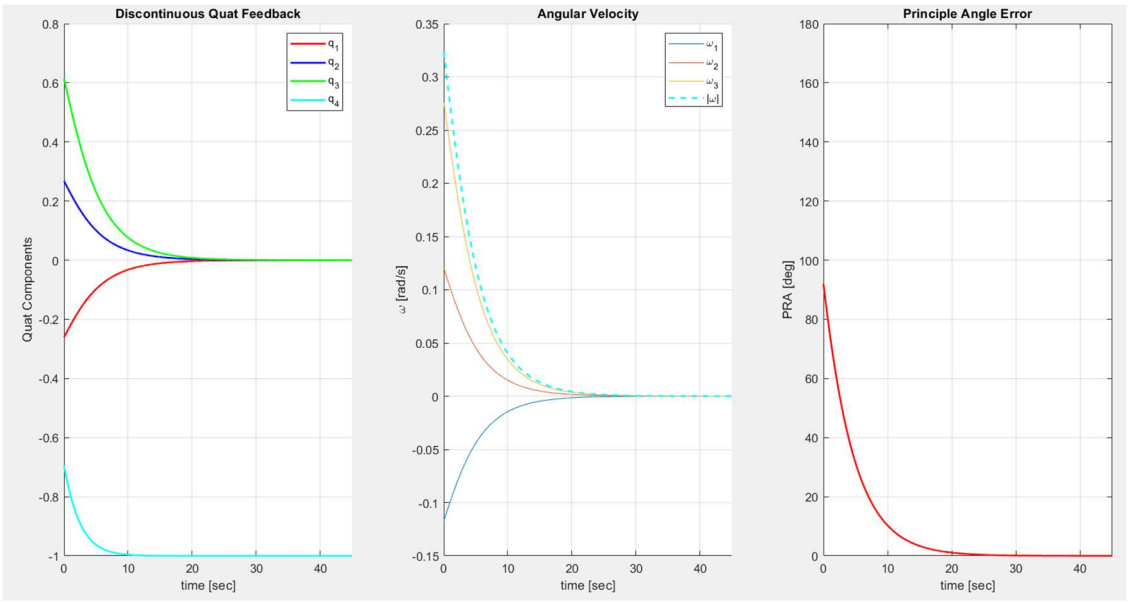

Figure 3: Discontinuous Quaternion Control

Figure 3 demonstrates the validity of the claims proposed in the methods section, the discontinuous control law prevents unwinding. The elimination of this problem also decreases the time for convergence of the identity attitude. This is far more practical and avoids energy waste, but the possible discontinuity at $q_4 = 0$ renders the control law imperfect. The angular velocity is identical to the quaternion vector components, with only a different magnitude attributed to the gain. The sign function in the control law returns -1 for negative q_4 which cancels the negative sign in the control law effectively handing the closed loop kinematics the vector quaternion scaled by the gain.

Lastly, the nonlinear control law, $\boldsymbol{\omega}_c = -kq_4\boldsymbol{q}$, aims to fix the problems presented by the linear and discontinuous control law. Moreover, the integration of the closed loop kinematics for this control law uses the same gain and initial conditions as previously.

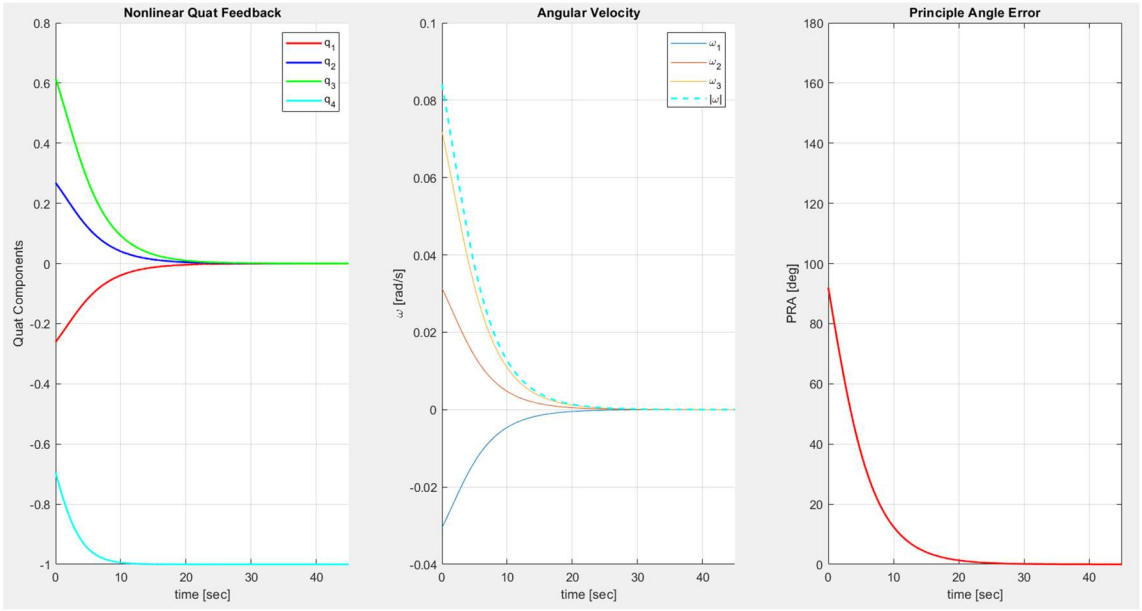

Figure 4: Nonlinear Quaternion Control

The nonlinear control law preforms very similar to the discontinuous control law, as predicted through Lyapunov's direct method the problem of unwinding is eliminated through the stability of both identity representations. The control effort (angular velocity) is orders of magnitude smaller than the previous laws. This comes from the q_4 term which will scale the control and is smaller for larger attitude errors. Using initial conditions with a negative q_4, the negative signs cancel in the control law and the scaled $\boldsymbol{q}$ is fed into the closed loop kinematics. The nonlinear control law produces a slightly slower response compared to the discontinuous control law but has a much lower cost. Each proposed control law is also tested with a range of initial conditions, and all stabilize identity attitude (Appendix B, Figure 16) with the exception of a $180°$ rotation for the nonlinear control law which through Lyapunov's direct method was concluded to not be in the region of attraction of stability for the control law.

MRP

Attitude regulation is performed with Modified Rodriguez Parameters using a 4th order Runge-Kutta integrator which switches to the shadow set at $|\sigma| = 1$ to avoid the singularities at $\pm 360°$. Two initial conditions are tested for each control law to properly analyze the behavior of the controllers. The scalar gain is set to $k = 0.65$ for all MRP cases.

$$IC(1): e = [1, -2, 3]\ \phi = 3\ (rad)$$
$$IC(2): e = [.25, -.86, .12]\ \phi = 0.8\ (rad)$$

Equation 29: Large(1) and Small(2) angle initial conditions

$$\sigma = \tan\left(\frac{\phi}{4}\right)\hat{e}, \hat{e} = \frac{e}{\|e\|}$$

Equation 30: Principle Angle/Axis to MRP Transformation

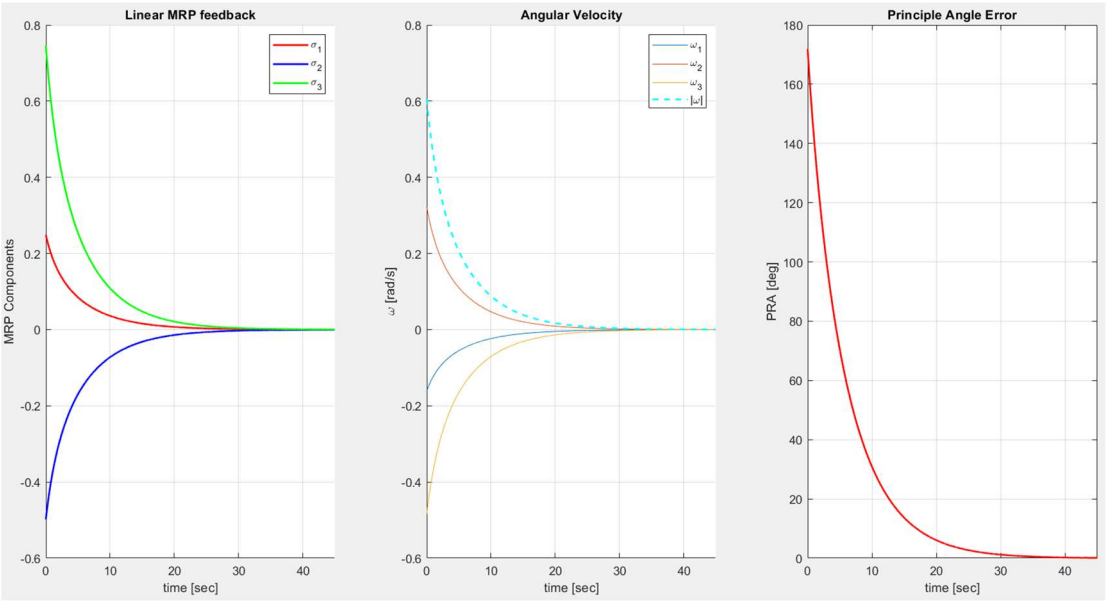

Figure 5: Linear MRP Control for Large Angle IC

Figure 5 demonstrates the stability of the linear feedback controller ($\boldsymbol{\omega}_C = -k\boldsymbol{\sigma}$) for the large initial angle, which as discussed is asymptotically stable. The control effort (angular velocity) is the

reflection of the MRP components scaled by the gain and is about $0.20\ rad/s$. As expected, the control effort is larger for larger attitude error.

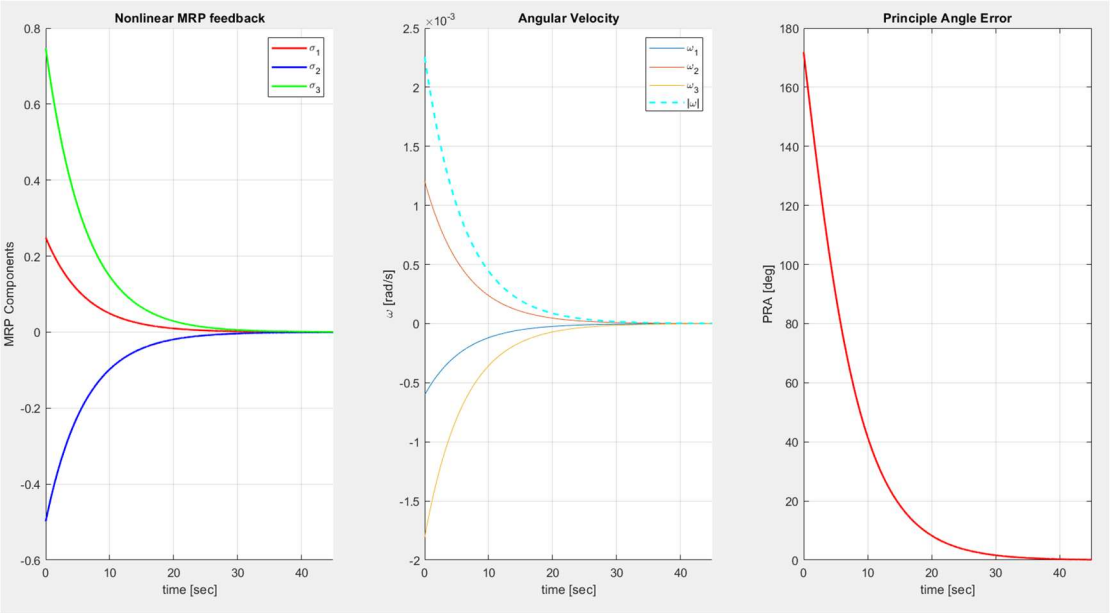

Figure 6: Nonlinear MRP Control for Large Angle IC

The response time for the nonlinear feedback controller is nearly identical to the linear feedback. Although the MRP regulation control constitutes the use of a 4th order Runge-Kutta integrator for switching to the shadow set, no such switch is seen even with the large angle initial condition. This is because the magnitude of σ starts below 1, and through attitude regulation it will never surpass 1 (Figure 7). Interestingly, the control effort (angular velocity) is much lower for the nonlinear control vs the linear. This is due to the structure of the nonlinear control law, which softens the control input for large σ values effectively normalizing large values of σ.

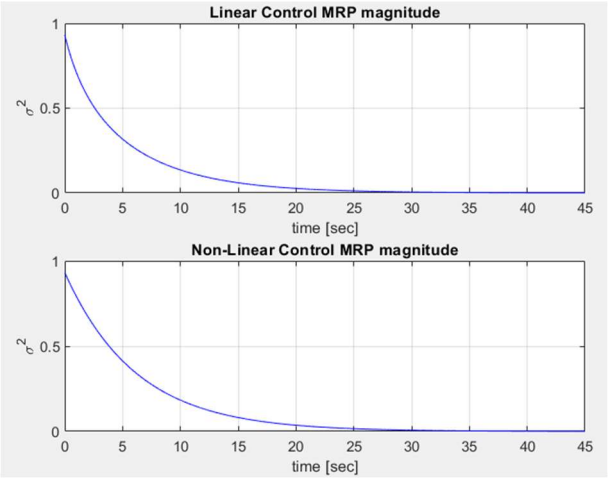

Figure 7: Magnitude of MRP vs Time for Large Angle IC

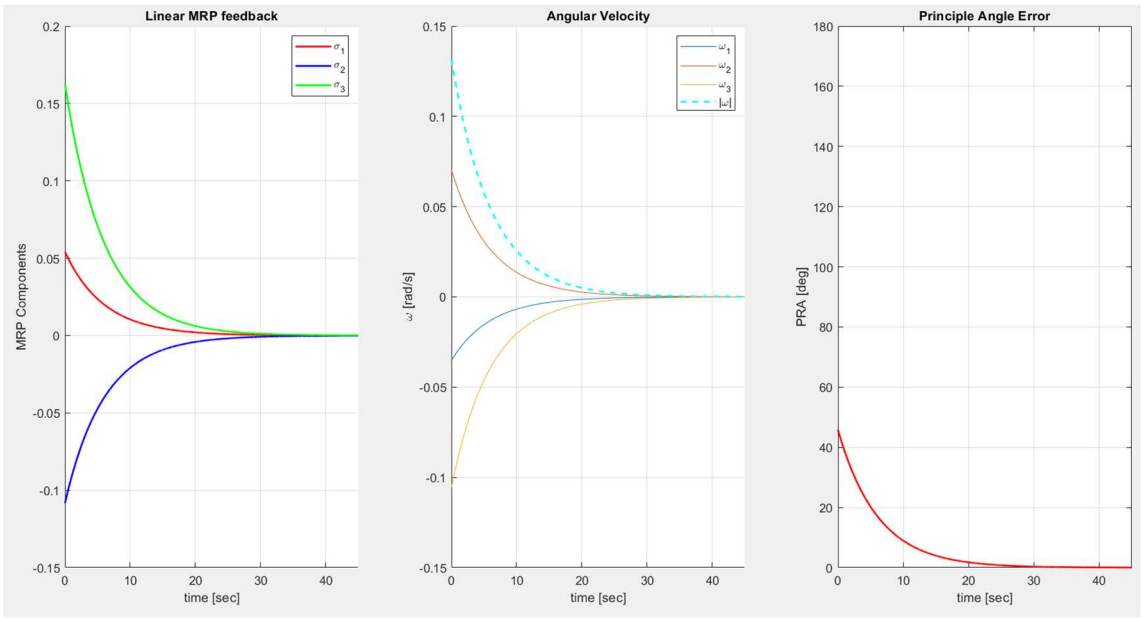

Figure 8: Linear MRP Control for Small Angle IC

IC(2) represents a rotation of $0.8\ (rad)$ about the same principle axis and is once again void of any shadow set switching in integration because the magnitude of σ never surpasses 1 (Figure 10). Again, the controller is asymptotically stable and comes to rest at the identity attitude as expected. The control effort is smaller in magnitude than experienced with the larger initial condition for the linear control. This is expected, as the controller is initially feeding smaller attitude error into the kinematics than for IC(1).

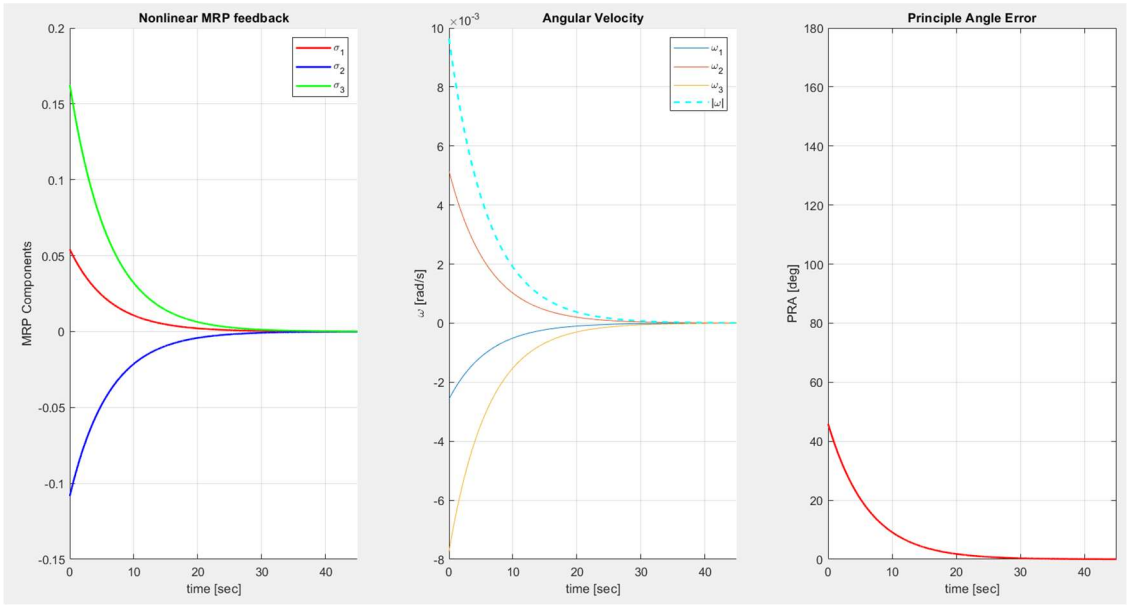

Figure 9: Nonlinear MRP Control for Small Angle IC

Comparable with IC(1), the response is almost identical for each controller, however the nonlinear controller has a much lower control cost (angular velocity). Again, this is attributed to the structure of the

nonlinear controller which effectively normalizes the control input. Both proposed control laws are tested with a range of initial conditions, which all stabilize at identity within 45 seconds (Appendix B, Figure 17)

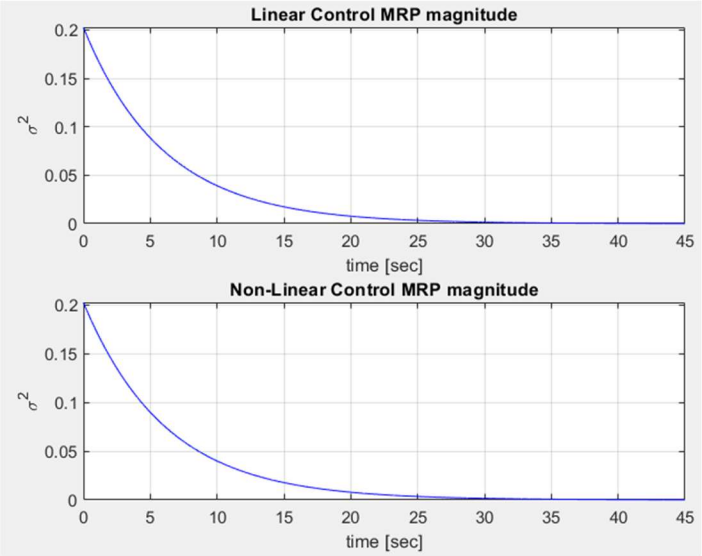

Figure 10: Magnitude of MRP vs Time for Small Angle IC

Task 2

Attitude Estimation

We compute the DCM's using the TRIAD method for various combinations of the given measurements as well as using the OLAE method. By evaluating the principle angle between DCM's, we determine relative trustworthiness of each measurement. We also compare the OLAE DCM to the DCM computed from measurements 1 and 2.

Applying the TRIAD and OLAE methods for each measurement pair yields the following DCM's:

$$[\hat{B}N_{12}] = \begin{bmatrix} 0.4156 & -0.8551 & 0.3100 \\ -0.8339 & -0.4943 & -0.2455 \\ 0.3631 & -0.1566 & -0.9185 \end{bmatrix}$$

$$[\hat{B}N_{13}] = \begin{bmatrix} 0.4167 & -0.8563 & 0.3051 \\ -0.8370 & -0.4924 & -0.2387 \\ 0.3546 & -0.1559 & -0.9192 \end{bmatrix}$$

$$[\hat{B}N_{14}] = \begin{bmatrix} 0.4279 & -0.8736 & 0.2317 \\ -0.8750 & -0.4646 & -0.1359 \\ 0.2263 & -0.1446 & -0.9633 \end{bmatrix}$$

$$[\hat{B}N_{OLAE}] = \begin{bmatrix} 0.4158 & -0.8548 & 0.3105 \\ -0.8352 & -0.4941 & -0.2416 \\ 0.3599 & -0.1588 & -0.9194 \end{bmatrix}$$

The corresponding principle angles are given in Table 4. Since the error is lowest when we omit measurement 4, it must be the least accurate measurement. Also note that the OLAE estimated DCM has the lowest error compared to the TRIAD estimated DCM from measurements 1 and 2.

Table 4. Principle Angles Associated with Each Set of Measurements

Measurements	2,4	3,4	2,3	2, OLAE
Principle Angle (Error), deg	7.7897	8.3194	0.5297	0.2312

Optimal Rest to Rest Maneuver

Applying the optimal rest to rest maneuver computed from the initial conditions defined by the OLAE estimated attitude for each axis results in the following Euler Angle and principle angle time histories. The prescribed maneuvers successfully drive the Euler Angles and principal angle to identity after 120 seconds, as shown in Figure 11. According to Figure 12, the principle angle changes the most to least during the 1 axis, 3 axis, then 2 axis maneuvers, corresponding to their relative difference from the identity state.

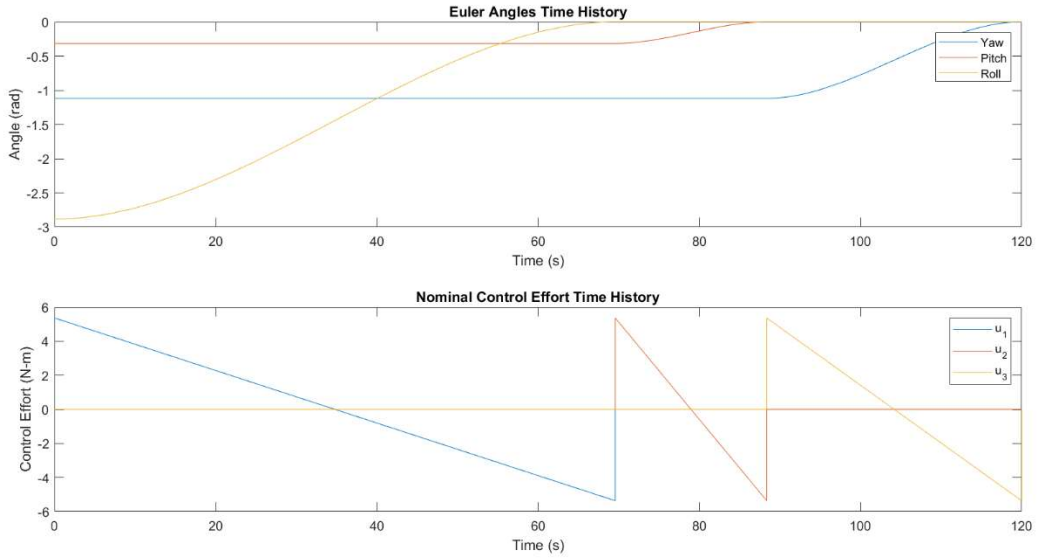

Figure 11. The nominal trajectories for the optimal rest to rest maneuver were computed to minimize control effort.

The maneuver times to correct each axis are given in Table 5, with larger maneuver times required to correct larger initial Euler Angles. A contour plot of the cost against maneuver times in Figure 20 of Appendix C validates our analytical solution. The total cost of the maneuver calculated from Equation 20 is $579\ N^2m^2s$.

Table 5. Maneuver Times for Total Reference Trajectory

Maneuver	1	2	3	Total
Maneuver time (s)	69.5747	31.6326	18.7927	120

Tracking Controller

To implement the tracking controller, an arbitrary natural frequency is chosen to be $\omega_n = 0.2$, corresponding to a scalar proportional gain of $k_p = 0.04$ and a scalar derivative gain of $k_d = 0.4$. However, to account for the spacecraft inertia properties we must multiply by the inertia matrix to obtain the gain matrices used in the feedback controller shown in Equation 31

$$k_p\boldsymbol{I} = \begin{bmatrix} 60 & 0 & 0 \\ 0 & 40 & 0 \\ 0 & 0 & 32 \end{bmatrix}, k_d\boldsymbol{I} = \begin{bmatrix} 600 & 0 & 0 \\ 0 & 400 & 0 \\ 0 & 0 & 320 \end{bmatrix}$$

Equation 31. The scalar gains multiplied by the inertia tensors produce gain tensors.

Comparing the perturbed Euler Angle time histories to their nominal time histories, we see that the perturbed trajectories track the nominal trajectories and reach zero within the 120 second time frame. The principle angle time history tells a similar story, where the perturbed principle angle follows the nominal trajectory and reaches zero at 120 seconds. We simulated time histories for initial Euler Angles

perturbed by up to 0.1 radians, and the controller drove all their states to identity as shown in Figure 19 of Appendix C. Thus, we constructed a critically damped PD controller for the spacecraft including its inertia properties and demonstrated that it drives the attitude to identity within 120 seconds despite a range of perturbations in the initial attitude.

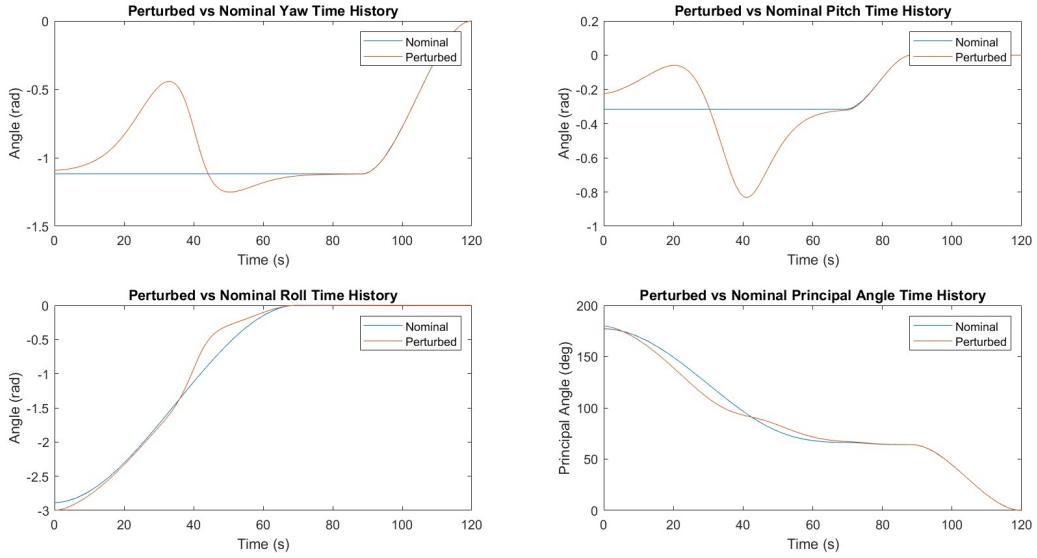

Figure 12. The PD critically damped controller successfully drives the spacecraft attitude to identity despite perturbations in the initial conditions.

Task 3

Control on $SO(3)$ demonstrates value due to its direct handling of the rotation matrix and its lack of singularities. The control law, $\boldsymbol{\omega}_c = -kS_A(R)$, was theorized to be almost globally asymptotically stable for the identity, with the unstable equilibria not included in the region of attraction. Through initial conditions in terms of 3-2-1 Euler angles ($\psi_0 = 100°, \theta_0 = 60°, \phi_0 = 30°$) and a control gain of $k = 0.05$, the stability hypothesis is tested through integration using a variational integrator.

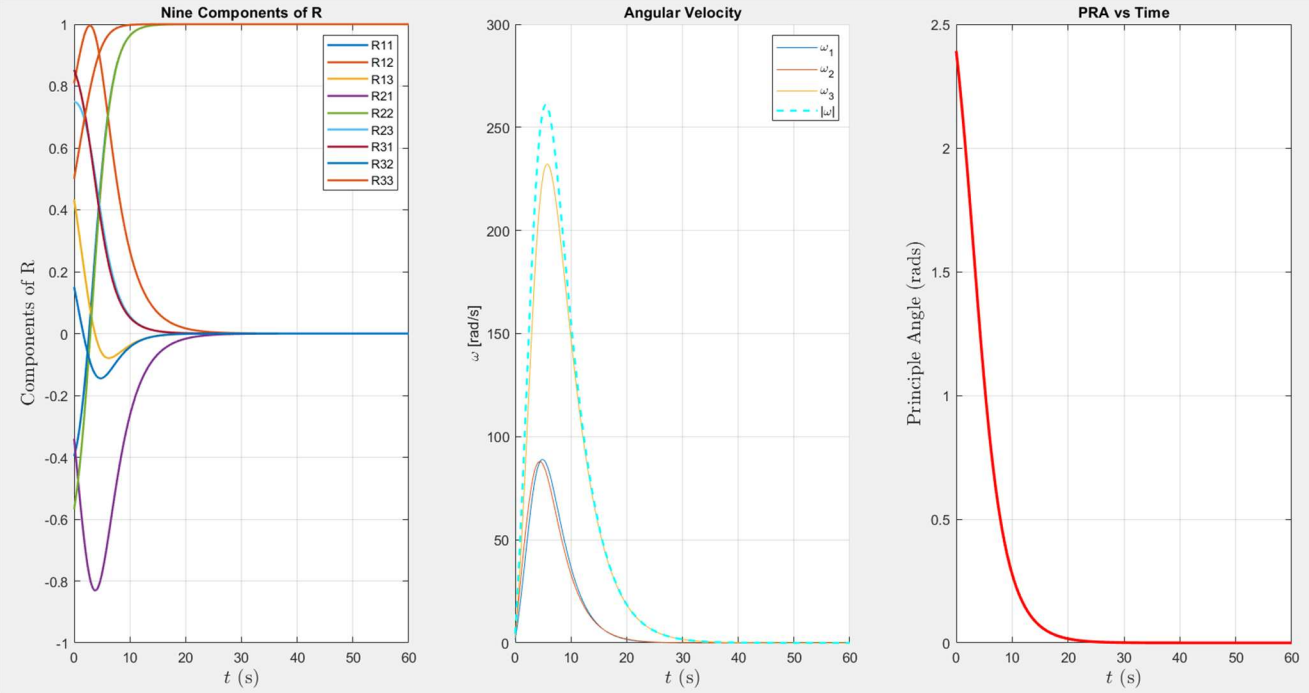

Figure 13: SO(3) Control

The controller successfully stabilizes the attitude at identity (Figure 13). The use of the variational integrator maintains orthogonality of the rotation matrices as well (Figure 14). The control is quite costly, with the magnitude of the angular velocity peaking around 260 radians per second. This is due to the linear proportional structure of the control law returning very large angular velocity for large errors in attitude from the identity.

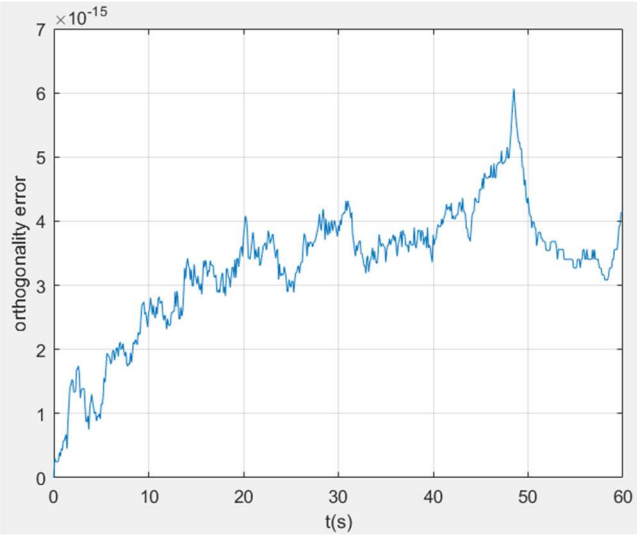

Figure 14: Variational Integrator Orthogonality Error

As discussed previously in the methods, the Morse-Lyapunov function has three unstable equilibria which are not a part of the region of attraction for the controller. These saddle points are seen in a mesh grid plot of the function (Appendix B, Figure 18). The points represent rotations by $180°$ and constitute a set of measure zero on SO(3) [3].

Conclusion

Through the numerical integration of the closed loop kinematics of multiple control laws, we conclude that Lyapunov's direct method is a valid process for analyzing a control law. The linear PRV control law converged within 20 seconds to the identity attitude. Amongst the control laws discussed for quaternions (linear, discontinuous, and nonlinear), the nonlinear control law proved to be the most efficient and prevented unwinding. The linear control law is flawed because it only stabilizes one identity representation and can exhibit unwinding with certain initial conditions. Although the discontinuous control law did not exhibit unwinding, it is undesirable due to the discontinuous control and the chance that sensor chatter may keep the attitude at an undesired spot with certain initial conditions. Both MRP control laws were tested with two initial conditions, large and small angle rotations. Both rotations tested are void of shadow switching because the magnitude never reaches the switching surface. The nonlinear controller exhibited a much smaller control effort than the linear counterpart in both cases, this is due to the structure of the nonlinear control law normalizing large values of $\boldsymbol{\sigma}$.

By applying the TRIAD and OLAE attitude estimation methods, we compute several different estimates for the initial attitude of a spacecraft and discuss the accuracy of each sensor measurement based on the principle angle between each attitude DCM. In doing so, we find that measurement 4 is the least accurate. Using the OLAE estimated attitude, we construct a series of single axis optimal maneuvers that drive the spacecraft to identity. The Linear Time Invariant system has the Kinematic Differential Equation for Euler angles in the system matrix and the inverse Inertia matrix in the control matrix. We compute the trajectory of the optimal rest to rest maneuver for each axis using the initial Euler Angles. Finally, we form a critically damped PD controller by picking scalar gains $k_d = 0.4$ and $k_p = 0.04$ and multiplying by the inertia matrix. When applied to a perturbed initial attitude, the PD controller successfully tracks the reference trajectory and drives the spacecraft to identity.

Through Lyapunov's direct method, the Morse-Lyapunov function for the SO(3) control law was concluded to be almost globally asymptotically stable excluding three unstable equilibria. This conclusion was validated through the numerical integration of the KDE using a variational integrator which preserves the orthogonality and properness of the rotation matrices. The controller successfully stabilizes the identity attitude within one minute from an arbitrary initial condition defined through 3-2-1 Euler angles. The cost of this controller, however, is very high. The control effort is very high when the attitude error is high, this comes from the control law feeding back the term $S_A(R)$ which tracks the error between the rotation matrix and the identity attitude.

References

[1] E. Butcher, "554: Lecture 9b Nonlinear feedback control," University of Arizona, Tucson, AZ, 2025.

[2] E. Butcher, "554: Lecture 6 Quaternions," University of Arizona, Tucson, AZ, 2025.

[3] E. Butcher, "554: Lecture 10 Attitude kinematics control," University of Arizona, Tucson, AZ, 2025.

[4] E. Butcher, "554: Lecture 4 Kinematic Differential Equations," University of Arizona, Tucson, AZ, 2025.

[5] E. Butcher, "554: Lecture 5 Principle angle-axis," University of Arizona, Tucson, AZ, 2025.

[6] E. Butcher, "554: Lecture 7 Rodriguez Parameters," University of Arizona, Tucson, AZ, 2025.

[7] E. Butcher, "554: Lecture 11 Attitude Determination," University of Arizona, 2025.

[8] E. Butcher, "554: Lecture 8 Single Axis Control," University of Arizona, 2025.

[9] E. Butcher, "554: Lecture 2 Direction Cosine Matrix," University of Arizona, Tucson, AZ, 2025.

Appendix A: Detailed Lyapunov Stability Proofs

PRV Linear Control Law

$$V(\gamma_I) = 0$$

$$V(\gamma) = \gamma^T\gamma > 0,\ \forall\gamma \in \mathbb{R}\backslash\{\gamma_I\}\ \text{< Lyapunov Candidate, Radially Unbounded}$$

$$\dot{V}(\gamma) = 2\gamma^T\dot{\gamma} = -k\gamma^T\gamma < 0,\qquad \forall\gamma \in \mathbb{R}\backslash\{\gamma_I\}\ \text{< Lyapunov Function, Globally Asymptotically Stable}$$

Quat Linear Control Law

$$V(q_I) = 0\ \ , q_I = [0,0,0,1]^T$$

$$V(q) = (1-q_4)^2 + \|\boldsymbol{q}\|^2 = 2(1-q_4) > 0\qquad \forall q \in S^3\backslash(0,1)\ \text{< Lyapunov Candidate}$$

$$\dot{V}(q) = \frac{d}{dt}\big(2(1-q_4)\big) = -2\dot{q}_4 = \boldsymbol{\omega}_c^T\boldsymbol{q}$$

$$\boldsymbol{\omega}_c^T = -k\boldsymbol{q}^T$$

$$\dot{V}(q) = -k\|\boldsymbol{q}\|^2 < 0\qquad \forall q \in S^3\backslash(0,\pm1)\ \text{< Lyapunov Function, Locally Asymptotically Stable}$$

Quat Discontinuous Control Law

$$V(q) = (1-|q_4|)^2 + \|\boldsymbol{q}\|^2 = 2(1-|q_4|) > 0\qquad \forall q \in S^3\backslash(0,\pm1)\ \text{< Lyapunov Candidate}$$

$$V(q_I) = 0,\ \ q_I = [0,0,0,\pm1]^T$$

$$\dot{V}(q) = sgn(q_4)\boldsymbol{\omega}_c^T\boldsymbol{q}$$

$$\boldsymbol{\omega}_c^T = -ksgn(q_4)\boldsymbol{q}^T$$

$$\dot{V}(q) = -k\|\boldsymbol{q}\|^2 < 0\qquad \forall q \in S^3\backslash(0,\pm1)\ \text{< Lyapunov Function, Locally Asymptotically Stable}$$

Quat nonlinear Control Law

$$V(q) = \|\boldsymbol{q}\|^2 = 1 - q_4^2 > 0\qquad \forall q \in S^3\backslash(0,\pm1)\ \text{< Lyapunov Candidate}$$

$$V(q_I) = 0\qquad q_I = [0,0,0,\pm1]^T$$

$$\dot{V}(q) = -2q_4\dot{q}_4 = q_4\boldsymbol{\omega}_c^T\boldsymbol{q}$$

$$\boldsymbol{\omega}_c^T = -kq_4\boldsymbol{q}^T$$

$$\dot{V}(q) = -kq_4^2\|\boldsymbol{q}\|^2 < 0\qquad \forall q \in S^3\backslash\{(0,\pm1),(\boldsymbol{q},0)\}\ \text{< Lyapunov Function, Locally Asymptotically Stable}$$

MRP Linear Control Law

$$V(\boldsymbol{\sigma}) = 2\boldsymbol{\sigma}^T\boldsymbol{\sigma} > 0\qquad \forall\boldsymbol{\sigma} \in \mathbb{R}^3\backslash\{0\}\ \text{< Lyapunov Candidate, Radially Unbounded}$$

$$V(\boldsymbol{\sigma_I}) = 0\qquad \boldsymbol{\sigma}_I = [0,0,0]^T$$

$$\dot{V}(\boldsymbol{\sigma}) = 4\boldsymbol{\sigma}^T\dot{\boldsymbol{\sigma}} = \boldsymbol{\sigma}^T[B(\boldsymbol{\sigma})]\boldsymbol{\omega}$$

$$= \boldsymbol{\sigma^T}\big[\big(1-\big|\boldsymbol{\sigma^2}\big|\big)I_3 + 2\boldsymbol{\sigma}^\times + 2\boldsymbol{\sigma\sigma^T}\big]\boldsymbol{\omega}$$

$$= \big(1-\big|\boldsymbol{\sigma^2}\big|\big)\boldsymbol{\sigma^T\omega} + 2\boldsymbol{\sigma^T\sigma}^\times + 2\boldsymbol{\sigma^T\sigma\sigma^T\omega}$$

$$= \big(1-\big|\boldsymbol{\sigma^2}\big|\big)\boldsymbol{\sigma^T\omega} + 2(\boldsymbol{\sigma^T\sigma})(\boldsymbol{\sigma^T\omega})$$

$$= \boldsymbol{\sigma^T\omega} - (\boldsymbol{\sigma^T\sigma})\boldsymbol{\sigma^T\omega} + 2(\boldsymbol{\sigma^T\sigma})(\boldsymbol{\sigma^T\omega})$$

$$= \boldsymbol{\sigma^T\omega} + \boldsymbol{\sigma^T\sigma\sigma^T\omega}$$

$$= (1+|\boldsymbol{\sigma}|^2)\boldsymbol{\sigma}^T\boldsymbol{\omega}$$

$$\dot{V}(\boldsymbol{\sigma}) = (1+|\boldsymbol{\sigma}|^2)\boldsymbol{\sigma}^T\boldsymbol{\omega}$$

$$\boldsymbol{\omega} = -k\boldsymbol{\sigma}$$

$$\dot{V}(\boldsymbol{\sigma}) = -k(1+|\boldsymbol{\sigma}|^2)|\boldsymbol{\sigma}|^2 < 0\qquad \forall\boldsymbol{\sigma} \in \mathbb{R}^3\backslash\{0\}\ \text{< Lyapunov Function, Globally Asymptotically Stable}$$

MRP nonlinear Control Law

$$V(\boldsymbol{\sigma}) = 2\boldsymbol{\sigma}^T\boldsymbol{\sigma} > 0\qquad \forall\boldsymbol{\sigma} \in \mathbb{R}^3\backslash\{0\}\ \text{< Lyapunov Candidate, Radially Unbounded}$$

$$V(\boldsymbol{\sigma_I}) = 0\qquad \boldsymbol{\sigma}_I = [0,0,0]^T\ <$$

$$\dot{V}(\boldsymbol{\sigma}) = 4\boldsymbol{\sigma}^T\dot{\boldsymbol{\sigma}} = (1+|\boldsymbol{\sigma}|^2)\boldsymbol{\sigma}^T\boldsymbol{\omega}$$

$$\boldsymbol{\omega} = -k\boldsymbol{\sigma}/(1+|\boldsymbol{\sigma}|^2)$$

$$\dot{V}(\boldsymbol{\sigma}) = -k|\boldsymbol{\sigma}|^2 < 0\qquad \forall\boldsymbol{\sigma} \in \mathbb{R}^3\backslash\{0\}\ \text{< Lyapunov Function, Globally Asymptotically Stable}$$

SO(3) Control Law

$$V(R) = \frac{1}{2}tr(A - AR) > 0 \qquad \forall R \in SO(3)\backslash\{I_3, E_1, E_2, E_3\} < \text{Lyapunov Candidate}$$

$$V(I_3) = 0$$

$$\dot{V}(R) = -\frac{1}{2}tr\left(A\dot{R}\right) = -\frac{1}{2}tr(AR\omega^{\times})$$

$$Using\ Identity: tr(B\omega^{\times}) = \omega^T(B^T - B)^{\vee}$$

$$\dot{V}(R) = w^T\frac{1}{2}(AR - R^TA)^{\vee} = \omega^T S_A(R)$$

$$\omega^T = -kS_A(R)^T$$

$$\dot{V}(R) = -kS_A(R)^T S_A(R) < 0 \qquad \forall R \in SO(3)\backslash\{I_3, E_1, E_2, E_3\} < \text{Lyapunov Function, almost GAS}$$

$$E_1 = R_x(180°), E_2 = R_y(180°), E_3 = R_z(180°)$$

Appendix B

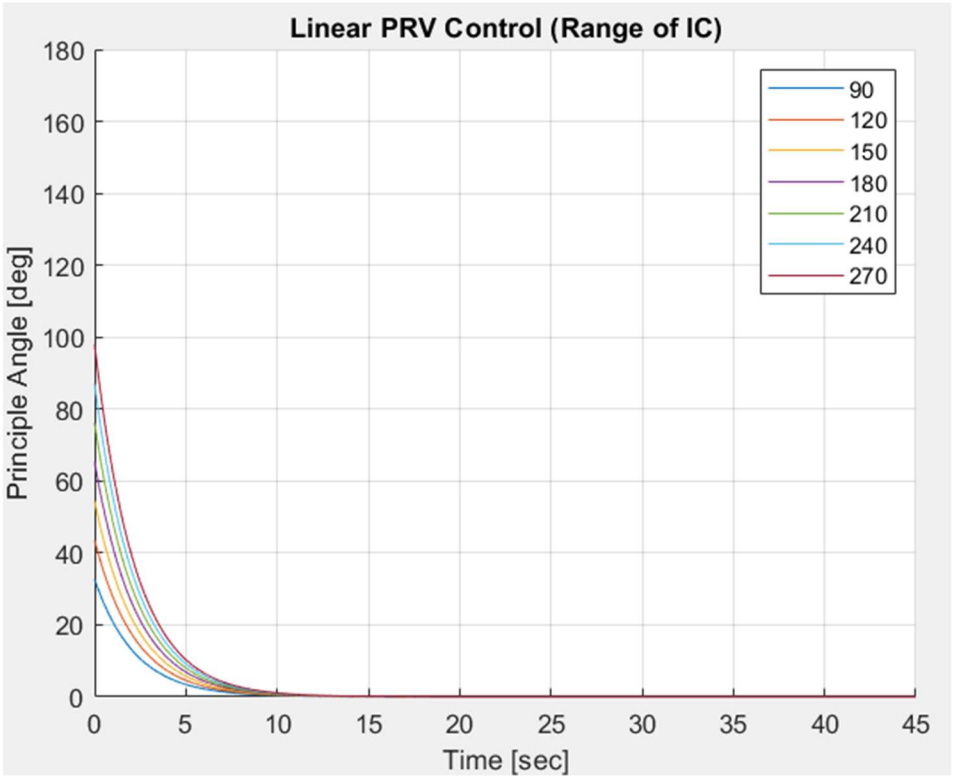

Figure 15: PRV Linear Control With Range of IC's

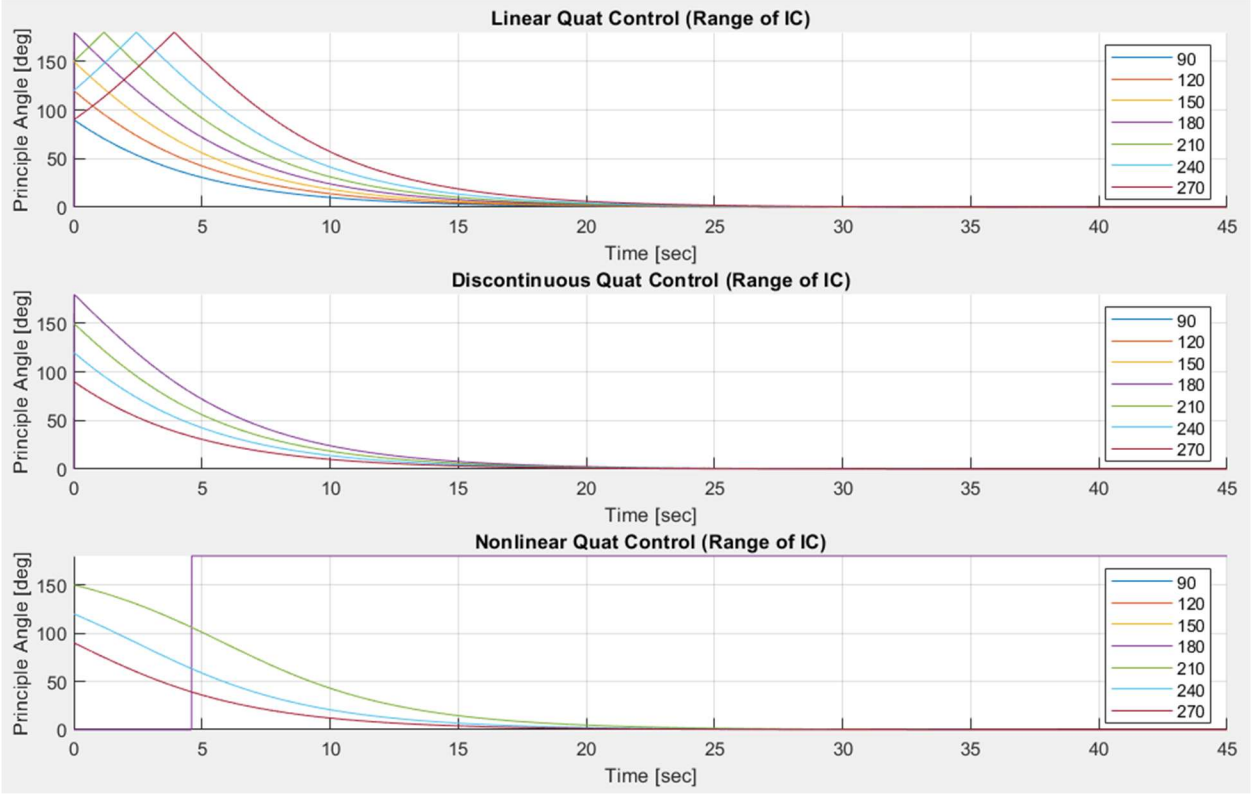

Figure 16: Quat Control With Range of IC's

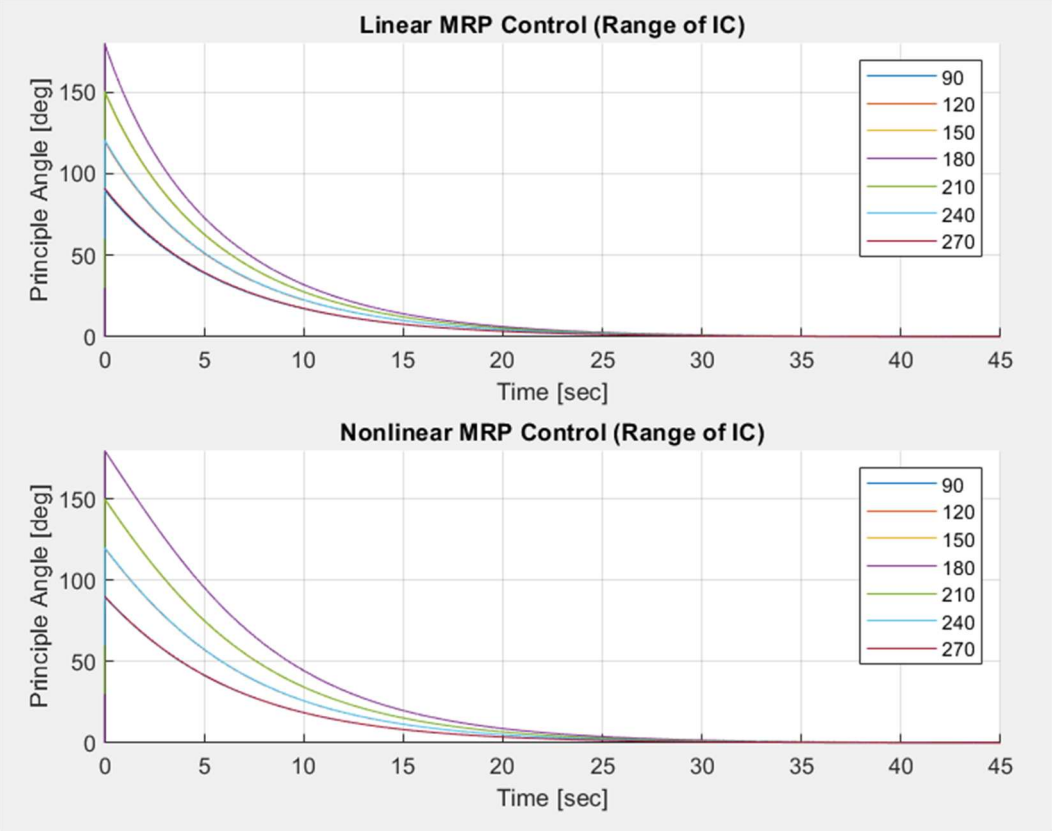

Figure 17: MRP Control With Range of IC's

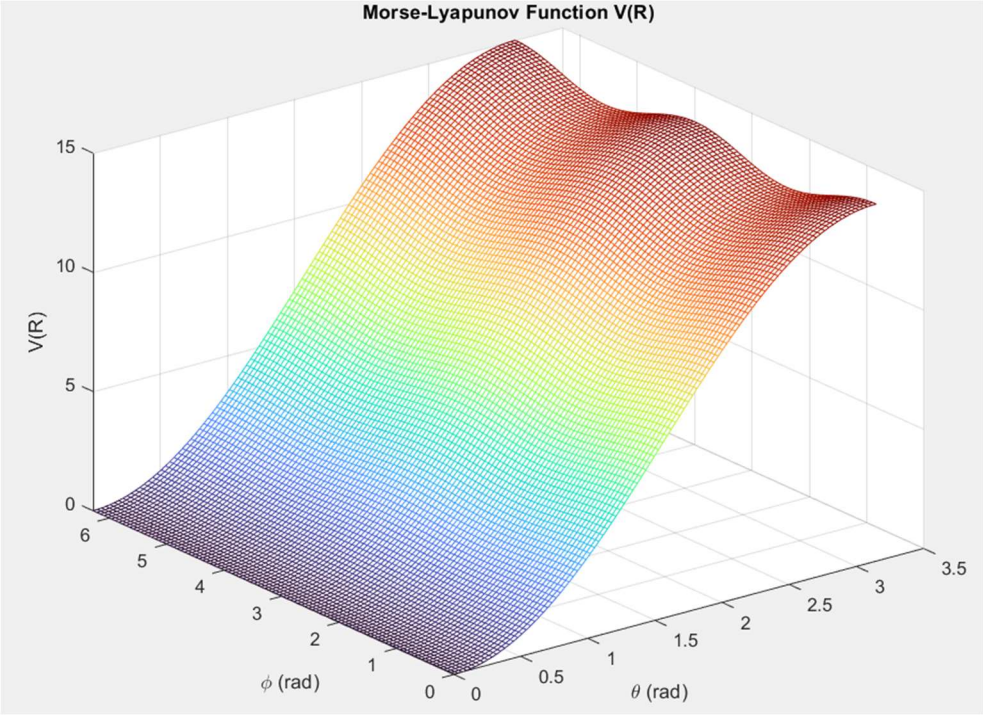

Figure 18: Morse-Lyapunov Function

Appendix C

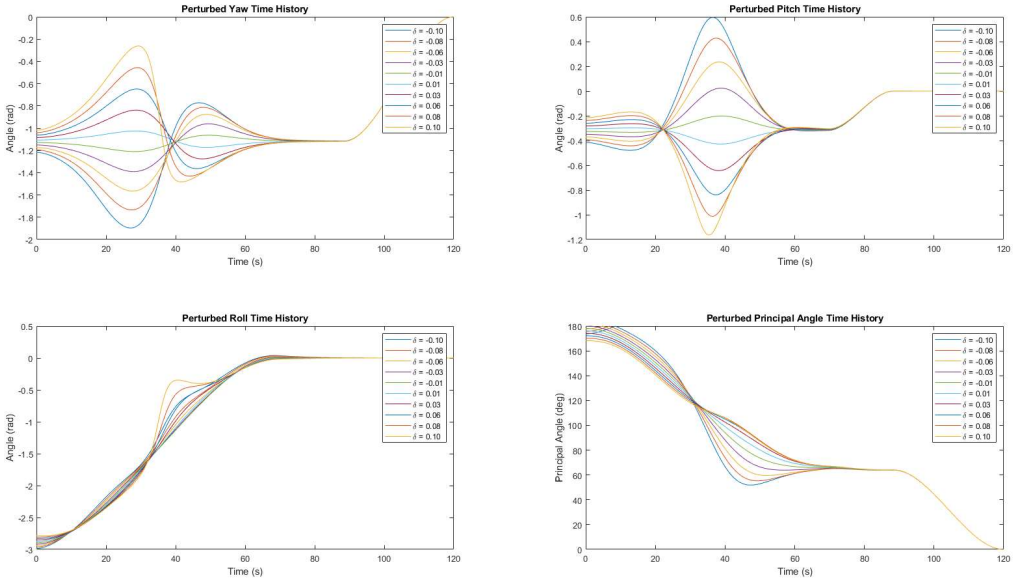

Figure 19. The tracking controller drives the attitude to identity given initial conditions that vary by ± 0.1 *radians.*

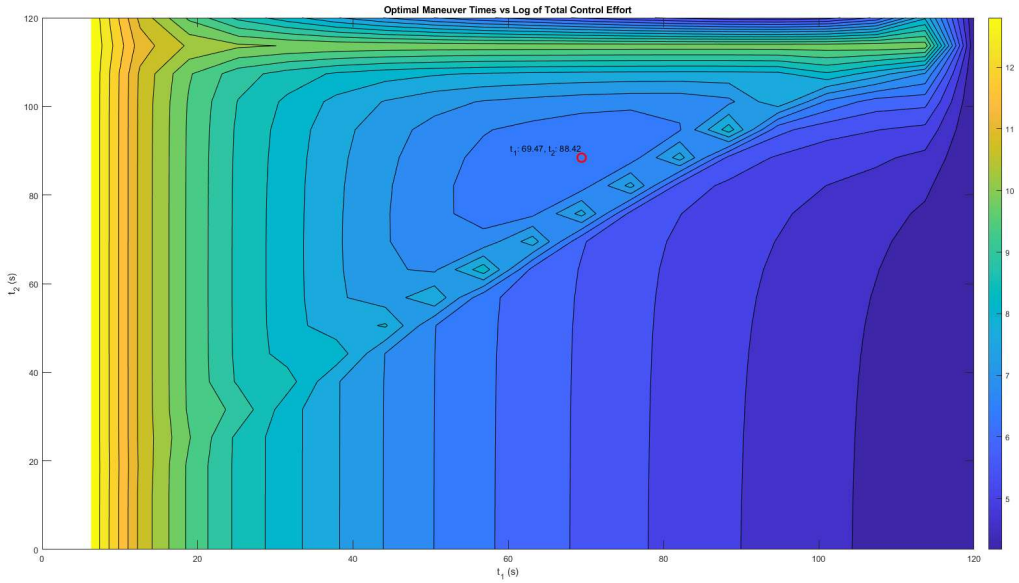

Figure 20. A contour plot of the cost function as it varies with maneuver times validates the analytical results. Note, we discard all solutions where $t_1 > t_2$*, since that is physically meaningless.*